Control Engineering Practice 72 (2018) 104–113

Contents lists available at ScienceDirect

Control Engineering Practice

journal homepage: www.elsevier.com/locate/conengprac

Development of a upper-limb exoskeleton robot for refractory construction

Ho Yu, Il Seop Choi, Kyung-Lyong Han, Jae Yeon Choi, Goobong Chung, Jinho Suh *

POSCO Technical Research Laboratories, Geodong-dong, Nam-gu, Pohang, Gyoengbuk, 790-300, Republic of Korea

ARTICLE INFO

Keywords:
Exoskeleton robot
Wearable robot
Power augmentation
Refractory construction

ABSTRACT

In this paper, a novel 7-DOF (degree-of-freedom) upper-limb robotic exoskeleton was developed for helping refractory construction operations in furnaces. The exoskeleton is the dual-arm type wearable robot that cooperates with human operators. Each arm includes Force/Torque (F/T) sensors to detect the human's motion, and the robot can handle a refractory of up to 50 kg. The exoskeleton robot generates not only high strength but also various 3-dimensional motions with the load, and it is highly suitable for the refractory construction operation.

1. Introduction

In the steel manufacturing industry, a multitude of heavy-weight handling processes exist. For instance, various transferring operations are required for delivering final products such as thick plates, wire rods, coils, etc. as well as half-finished products such as slabs, blooms, and billets. Except for steel products, numerous weight transporting operations of ladles, pressing rolls, steel scraps, steel specimens, and so on are performed. Relatively large and heavy materials described above cannot be handled by human power, and therefore overhead cranes and forklift trucks are largely utilized.

Meanwhile, there are multiple weight transferring works that can be handled by the human strength. A representative example is the refractory construction of the converter. The work is to pile up the refractory bricks inside the converter to delay erosion from the molten steel with high temperature. A number of complicated and unstructured activities such as aligning the bricks, inserting papers between bricks, etc. are required in this process, and thus human's intelligence and sense are absolutely important. Moreover, the limited working space inside the converter does not allow large and heavy facilities to be employed. Hence, the refractory construction of the converter cannot be fully automated and depends on both worker's muscle strength and a pneumatic air-balancer, which is a rather simple facility to lift and move the refractory bricks.

Fig. 1 illustrates the structure of the converter and photographs of the refractory handling operation in POSCO. Approximately thirteen thousands of refractory bricks that weigh 25–80 kg are piled up inside of the converter. Fifteen to twenty workers are involved in the construction, and it continues for four to six days. Dozens of times of refractory construction of the converter are performed annually in POSCO.

The converter is typically comprised of bottom, body, and cone parts as shown in Fig. 1(a). During the construction, air-balancers are utilized in the bottom and the body parts of the converter whereas the human strength is used in the cone part where the bricks are relatively small and light in Fig. 1(b). The air-balancer cannot be employed in the cone part due to the interference with the inner wall of the converter. However, thousands of refractory transferring operations in the cone part cause operators' musculoskeletal pains on back, waist, and wrists. Furthermore, the latent muscular skeletal disorder caused by handling heavy-load materials for a long time may generate severe safety accidents.

Exoskeleton robots recently have been developed extensively for helping and augmenting human's muscle strength. The powered robot is a wearable type robotic exoskeleton that cooperates with human operators. The robot utilizing electric or hydraulic actuators supports or augments human muscle strength to help transporting heavy-weight objects. This reduces the physical fatigue of operators from long hour of repetitive works with heavy loads, resulting in muscular skeletal diseases.

Up to now, a variety of exoskeleton robots have been designed and implemented. The first development of exoskeleton was started by General Electric and the United States military in the 1960s as the name of Hardiman. Mosher (1967) Since then, several exoskeleton robots have been developed for a variety of purposes in many organizations. For example, XOS series by Raytheon (0000) HULC by Lockheed martin (0000) and BLEEX from Berkeley (Huang, Steger, & Kazerooni, 2005; Kazerooni, Racine, Huang, & Steger, 2005) are primarily designed with military purposes. HAL by Cyberdyne (Hayashi, Kawamoto, &

* Corresponding author.
E-mail addresses: katen.yu@samsung.com (H. Yu), suhgang@kiro.re.kr (J. Suh).

http://dx.doi.org/10.1016/j.conengprac.2017.09.003
Received 29 October 2016; Received in revised form 3 September 2017; Accepted 4 September 2017
Available online 16 December 2017
0967-0661/

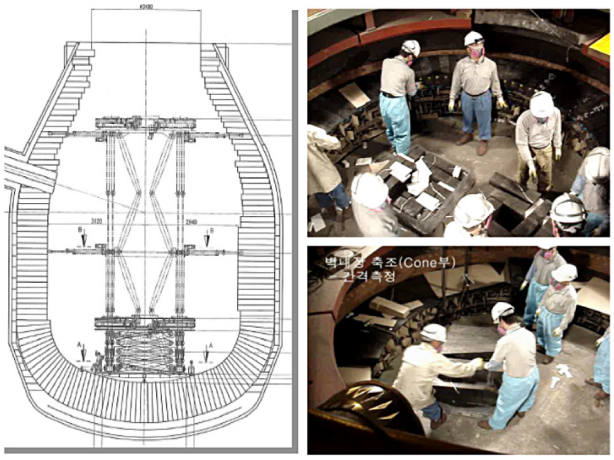

Fig. 1. Converter structure and photographs of the refractory construction.

Sankai, 2005; Kawabata, Satoh, & Sankai, 2009) and ReWalk by ReWalk robotics (0000) are developed for people with physical disabilities in heath cares. H-LEX by Hyundai motor group (Hyundai Motor Group, 0000), Daewoo Shipbuilding and Marine Engineering's exoskeleton at the shipyard (DSME, 0000), and FORTIS by Lockheed martin (0000) are the robot for industry. Nevertheless, most exoskeleton robots up to now have been focused on the military and rehabilitation purposes rather than industrial applications.

First, former exoskeleton robots were tried to apply in the refractory operation. Full-body type robots such as XOS, HAL and so on, which can manipulate refractories, were considered. The locomotion with legs like human can move well, but those platforms were vulnerable to maintain a balance against abrupt change of mass center when lifting heavy loads. Therefore, a more reliable robot mover was required instead of the leg frames.

In this paper, a novel dual-arm type upper-limb exoskeleton combined with air-balancer was developed for helping the refractory construction in the converter. Each arm includes a F/T sensor for detecting the human's motional intension accurately, and this allows to achieve delicate motions while handling weights. Moreover, various control algorithms combined with sensors enables operators to handle a refractory up to 50 kg with ease and secure their safety during the operation.

The applicability and stability of the robot system were focused to be improved for steel industry comparing to preceding robots. The upper-limb robot can be simply installed at the end-effector of the air-balancer, which is currently used in the bottom and body part of the refractory construction. By use of the exoskeleton robot, the air-balancer can be used in the cone part of the converter. In addition, the combination of the upper-limb exoskeleton robot and the air-balancer can provide safe and stable refractory transferring operation. There are no concerns for a wearer to fall down while working because air-balancer securely holds the robot and wearer, although rapid change of mass center caused by the refractory occurs.

2. Motion analysis

The motion analysis of refractory handling works was performed to determine a concept of the upper-limb exoskeleton such as joint mechanism, operational range, joint velocity etc.

In transporting a heavy object, various joints and muscles on shoulder, arms, and back in the upper body are used. The representative joint mechanism of the human's upper body reflected to the design of robotic exoskeleton is specifically constructed as shown in Fig. 2, where the mechanism consists of shoulder, elbow, and waist joints. In detail, the shoulder includes flexion, abduction, and rotation. The elbow has only flexion, and the waist has rotation, flexion and lateral flexion.

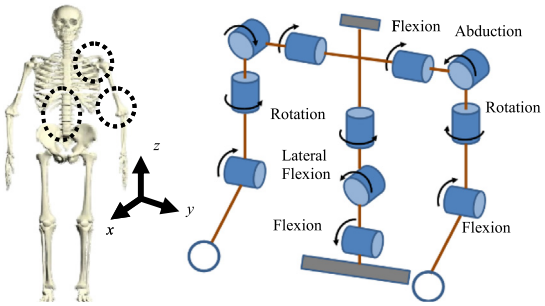

Fig. 2. Upper-body joint mechanism of the human body.

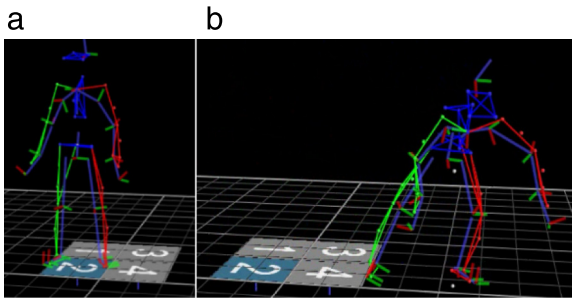

Fig. 3. Motion simulation by Vicon camera system: (a) refractory lifting and (b) transferring.

Table 1
Joint rotation angles.

Joint	Direction	Human range	Robot range
Elbow	Flexion	40–90°	60–160°
Shoulder	Flexion	−10~50°	−80~70°
	Abduction	20–90°	–
	Rotation	−60~30°	−90~3°
Waist	Flexion	−10~30°	0–60°
	Lateral flexion	−25~25°	–
	Rotation	−10~10°	–

The refractory handling operations are generally classified as several motions such as: (i) a vertical transport that lifts the refractory from low position to near waist, (ii) a horizontal transport that moves the refractory to other places in parallel with the ground, (iii) a rotation of the refractory for proper positioning, (iv) a walking motion with a refractory, (v) several other minor works such as refractory cutting, aligning, and position fixing, etc.

There are two common types of refractory moving activities. One is the horizontal transferring without moving the lower body as a short-range construction. The upper body moves to the right and left directions with waist bending resulting in generation of fast flexion and extension motions on elbows. The other is the refractory transferring with walking as a 2–4 steps distance. This includes the waist bending, but the horizontal movements of both arms are small. Hence, relatively slow flexion and extension motions on elbows are generated.

Based on the motions above, we simulated the refractory transferring operation by Vicon motion capture camera in Fig. 3 (Vicon, 0000). The refractory handling motion containing relatively large upper-body movements was considered.

As for an example of the motion analysis, Fig. 4 presents trajectories of left and right hands with respect to the waist joint. Both arms approximately move in the range of 500 mm, 1000 mm, 400 mm in x, y, z, respectively. Each joint rotation of the upper body is presented in Table 1. The result may vary depending on the operator who performs the refractory transport.

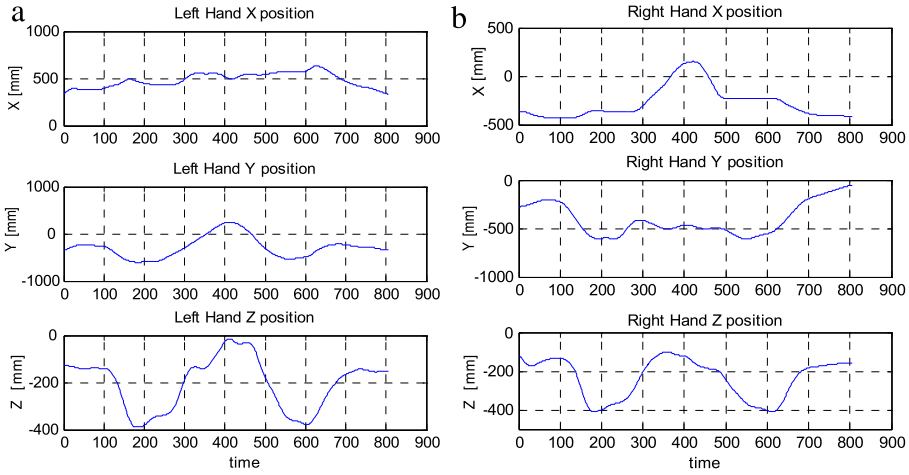

Fig. 4. Trajectories of both hands with respect to the waist joint: (a) left hand and (b) right hand.

It was shown that the transferring mechanism with the exoskeleton is slightly different from the refractory handling by humans, because the robot can compensate for a weight and the robot handles a refractory via a specific gripper, whereas human carries the weight by hand directly. For instance, the upper-limb robotic exoskeleton does not include all joints shown in Fig. 2. Refractory construction with aid of the exoskeleton requires no abduction on shoulder, rotation and lateral flexion on waist, where these joints were not considered in the design of the robot. when a person lifts and transfers a heavy object, the abduction movement of the arm was often used because the waist could not be turned much. However, this movement is not necessary in the robot operation because the robot can move freely around the waist. The robot does not need to generate fast speed like human since it does not use the counteraction as well. Therefore, it was concluded that the robot can transfer a heavy refractory even if there is no open shoulder (abduction) movement in both sides.

Besides, it was more crucial factor in design status that the robot would be light enough for people to handle it easily. In the case of the shoulder, for instance, we could not apply all three joints because of the limitation of space and the robot mass. Thus, only essential shoulder joints specialized for the refractory transfer operations were designed. Instead, additional gait and turning motions were provided by the air-balancer. Hence, the DOF of the upper-limb was reduced to 7.

The robot joint movement was determined within a range that does not interfere with the operator's movement based on the motion analysis. The robot movement is not coincident with the human motion, because the position of joints are different. The joint movement range is primarily limited by the software and secondary mechanical stoppers limit the movement for safety in Table 1.

3. Mechanical design

Motions of each part of the human body while transferring refractories in the converter were analyzed. The information of required motions, joint moving ranges, and joint torques for the refractory construction were acquired. Based on the motion analysis data, actuators on the body frame were designed.

3.1. Overall design

The weight of refractory in the cone part of the converter is 25–50 kg. Since most of refractories in the cone part weigh around 30–40 kg, a nominal payload of the robot exoskeleton should be at least 40 kg for proper refractory transferring operations. In addition, the rotational velocity of each joint needs a fast and sensitive enough motion for workers not to feel physical fatigue due to the robot.

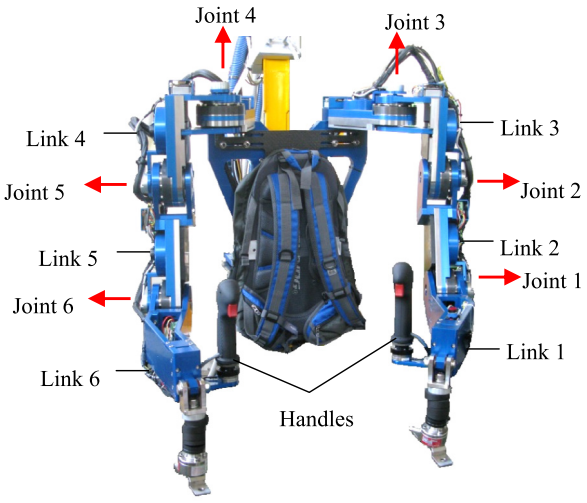

Fig. 5. Photograph of the upper-limb wearable robot exoskeleton.

Fig. 5 shows the photograph of the upper-limb wearable exoskeleton robot. The robot performs refractory lifting and transferring operation using 7 electrical joint actuators. Each arm includes three active joints and an additional back joint was installed for the waist bending. Elbow joints (joint 1 and joint 6) and vertical shoulder joints (joint 2 and joint 5) are involved in lifting the refractory and horizontal shoulder joints (joint 3 and joint 4) perform the refractory transferring motion in parallel with the ground. Handles includes 6-axis F/T sensors and a toggle switch to control dual-arm motions and the bending motion, respectively.

Since the robot has the overall weight of 72.4 kg and does not have the lower body that can provide the moving ability, the upper-limb solely cannot be used for refractory handling due to the robot weight. In order to replace the lower body, we proposed the combination apparatus of an air-balancer and the upper-limb exoskeleton robot in Fig. 6. Basically, the air-balancer uses the pneumatic cylinder to generate anti-gravity force and provides free horizontal motions with passive joints. By connecting the upper-limb exoskeleton at the end-effector of the air-balancer, the exoskeleton robot can move freely at the work site. Since the air-balancer is used in the construction of the bottom and body parts of the converter, no additional equipments such as the lower-limb or wheels are required to apply the upper-limb exoskeleton in the cone part construction.

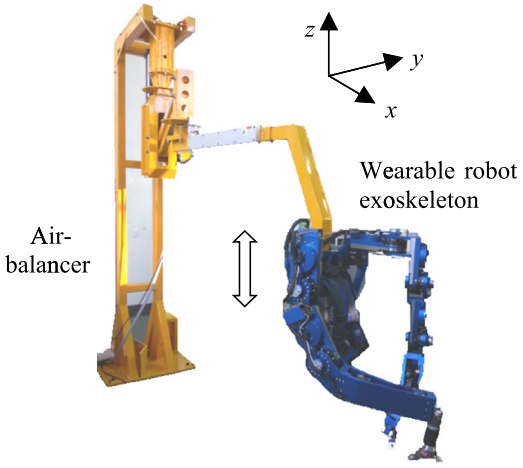

Fig. 6. Combination of the exoskeleton robot and the air-balancer.

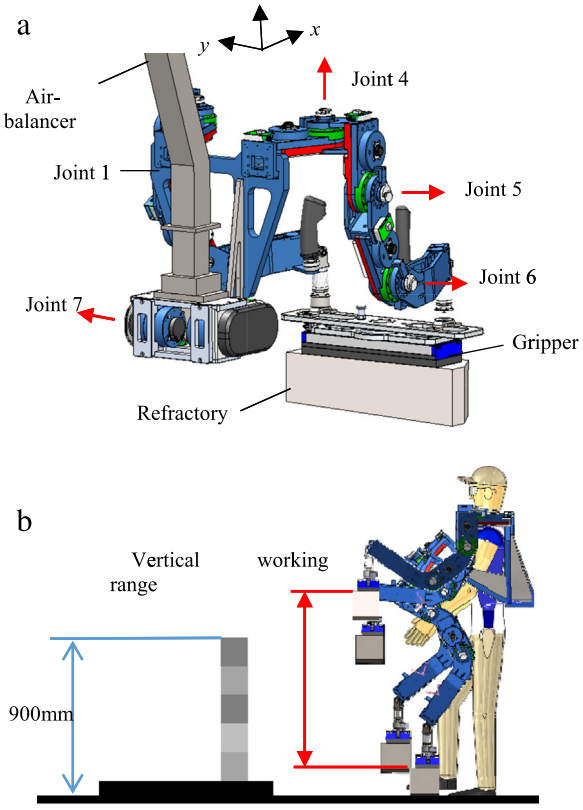

Fig. 7. CAD model (SolidWorks) of the upper-limb exoskeleton: (a) rear view and (b) vertical movement.

Concerning motions of refractory construction, lifting, transporting, and rotation of the refractory in a small range are performed in the exoskeleton robot while the horizontal movement through the gait in a relatively large range is operated by the air-balancer.

The vertical motion, which performs the refractory lifting and putting down, is generated by the vertical shoulder actuators (joint 2, 5), elbow actuators (joint 1, 6), and waist actuator (joint 7) in Figs. 5 and 7(a). The movement range to lift the refractory in the vertical direction is illustrated in Fig. 7(b). Piles of refractories on pallets are provided from the entrance of the converter to the construction position. The robot exoskeleton can handle the refractory in the level of 1–5 with the aid of the waist actuator (joint 7). Heights of the pallet and the refractory

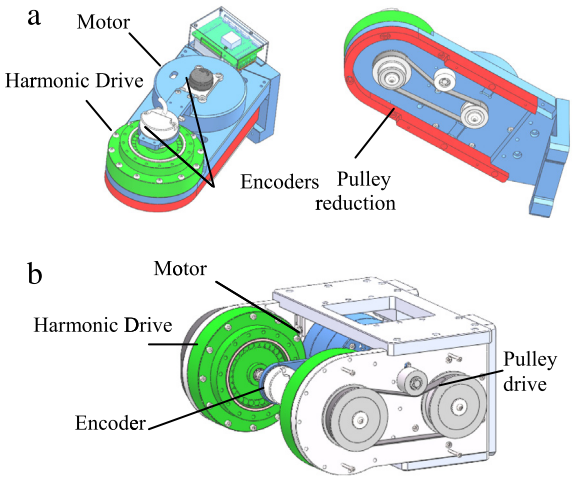

Fig. 8. Joint actuator modules: (a) an actuator module for joint 1–6 and (b) an actuator module for joint 7.

are both 150 mm so that the top position of the refractory is around 900 mm distance from the ground.

The horizontal motion, which transfers the refractory left or right in xy-plane, is provided by horizontal shoulder actuators (joint 3 and 4) in Figs. 5 and 7(a). In addition, the passive joint between the air-balancer and the upper-limb exoskeleton supplies the rotation motion of the whole robot frame. The operator who wears the robot exoskeleton can walk around using the air-balancer.

3.2. Actuation part design

Since the target payload of the upper-limb exoskeleton is maximum 50 kg, a single arm should be designed to support the load of 25 kg. The largest length of moment-arm was regarded as 0.461 m from shoulders (joint 2 and joint 5) to the end-effectors in the posture of the operator's maximum payload lifting. As a result, the required torques on the shoulder (joint 2 and joint 5) and elbows (joint 1 and joint 6) are calculated as follows.

For instance, the elbow joint on the left needs the following actuation torque to lift the refractory of 25 kg.

$$M_1 \times 0.426\ \text{m} \times 9.81\ \text{m/s}^2 = 126.83\ \text{Nm}, \tag{1}$$

where M_1 is 30.35 kg that is the total weight of the refractory, tool, and link 1. The shoulder joints also require actuation torque as follows,

$$M_2 \times 0.423\ \text{m} \times 9.81\ \text{m/s}^2 = 146.68\ \text{Nm}, \tag{2}$$

where M_2 is 35.35 kg that includes M_1, joint 1 actuator module, and link2. Based on the required joint torques above, the actuator modules were designed as shown in Fig. 8(a). The specification of the apparatus including electrical motors and Harmonic Drives is introduced in Table 2, where the safety factor of 20% was considered.

The actuator module in Fig. 8(a) is comprised of the motor, Harmonic Drive, encoders, and pulley reduction. This generates theoretically 269.28 Nm peak joint torque at each joint, which satisfies the required torques of shoulders and elbows. The same actuator modules were used in six joints except the waist joint in order to have a big advantage concerning the device maintenance. The motor and the Harmonic Drive are connected by the pulley reduction gear in Fig. 8(a).

The pulley mechanism between the motor and the reducer allows the easy arrangement of devices and a natural shape of the body frame without protrudes of devices. In addition, the gear ratio can be easily changed in accordance with the required torque by varying the number of teeth of the pulley sprockets.

Table 2
Specification of actuators.

Joint	Motor & Reducer	Rated torque	Peak torque	Link	Joint speed
1	SHG25 RBE 02110C	190.29 Nm	269.28 Nm	450 mm 4.8 kg	30.6 rpm
2	SHG25 RBE 02110C	190.29 Nm	269.28 Nm	270 mm 5.0 kg	30.6 rpm
3	SHG25 RBE 02110C	190.29 Nm	269.28 Nm	100 mm 4.7 kg	30.6 rpm
4	SHG25 RBE 02110C	190.29 Nm	269.28 Nm	100 mm 4.7 kg	30.6 rpm
5	SHG25 RBE 02110C	190.29 Nm	269.28 Nm	270 mm 5.0 kg	30.6 rpm
6	SHG25 RBE 02110C	190.29 Nm	269.28 Nm	450 mm 4.8 kg	30.6 rpm
7	SHG32 RBE 02111C	223.16 Nm	343.72 Nm	300 mm 43.4 kg	16.04 rpm

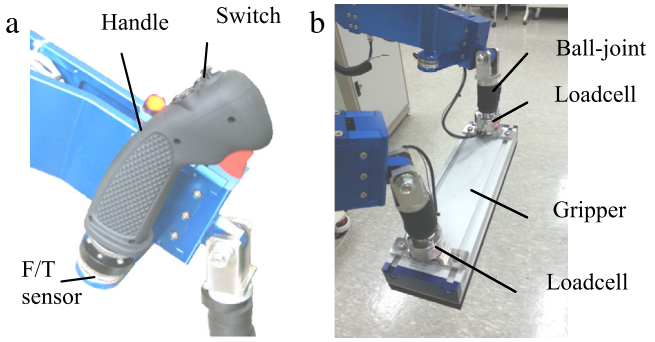

Fig. 9. Photographs of the handle and the gripper: (a) the handle and (b) the gripper.

The maximum target payload for the waist actuator (joint 7) is around 102.3 kg, which includes the refractory, the robot frame, and tool except the waist actuator of 25.1 kg. The largest length of moment-arm while lifting was considered as 0.486 m from the waist joint to the center of mass. The maximum required actuation torque on the waist joint can be calculated as follows,

$$M_3 \times 0.486\ \text{m} \times 9.81\ \text{m/s}^2 = 487.73\ \text{Nm}, \tag{3}$$

where M_3 is the maximum target payload. The actuator in joint 7 generates peak torque of 343.72 Nm, which requires dual actuator modules in parallel to support the maximum payload in Fig. 8(b).

Fig. 9(a) illustrates a handle located at the end position of each arm. A six-axis F/T sensor is installed at the bottom of the handle and measures operator's motion intension. From the direction and the magnitude of human force measured by F/T sensors, desired torque inputs are generated and transferred to each joint. The waist joint, on the other hand, is controlled by the switch at the top of the handle.

The large area vacuum gripping system (Schmalz FMC-SW 435.5/18) was applied to a refractory gripper in Fig. 9(b). This system guarantees high reliability and flexibility with high suction force in refractory absorption. Moreover, the refractory can be handled with at least 60% of contact area between the material and the suction pad. Also, there is no sliding phenomenon though the gripper is tilted. The insertion of ball-joint at the end-effector increases the degree-of-freedom of the gripper. The rubber pad housings around the ball-joint provide a proper damping. A pair of load cells between the ball-joints and the gripper measure the weight of the load in real-time for the robot control. Table 3 presents the part list of the upper-limb robot exoskeleton.

4. Control

Since the exoskeleton robot is a human–machine interacted system, it should not impose fatigue on the operator due to the asynchronism. In other words, the robot needs its fair enough dynamic performances with respect to the human's working motions. Nevertheless, the exoskeleton does not require a high level controller such as non-linear model-based controllers, because the human–machine collaborated robot can control its motion, force, and velocity by utilizing operator's intelligence and senses. Moreover, the refractory transferring does not need precise positioning and high-speed moving operations. Therefore, a rather simple and robust velocity tracking torque control can show good performances.

Table 3
Part list.

Part	Model	Manufacturer	Number
Motor driver	WHI 20/60	ELMO	7
Incremental encoder	E8P-512-276-D-D-M-B	US digital	8
Absolute encoder	RM44SC0013B10F2E1	RLS	7
Force/Torque sensor	ATI MINI40	ATI	2
Loadcell	CDES-50	Bongshin	2
Gripper	FMC-SW 435.5/18	Schmalz	1
Vacuum pump	EVE-tr 10 ac	Schmalz	1

4.1. Velocity tracking torque control

In the robot position control using F/T sensors, the controller generally requires high gains. This causes excessively sensitive responses against the sensor noise so that the severe vibration occurs occasionally in human-machine interacted system. Hence we applied the velocity tracking torque control instead of the position based control to achieve robust performances.

The basic control scheme of the upper-limb exoskeleton is to operate dual robot arms in the desired position and force by recognizing the operator's motion intension. The F/T sensors installed at each arm measure the magnitude of the human force and its direction. Meanwhile, the waist joint motion is derived from the input signal of a switch on the handle. Based on these signals, the 7-DOF upper-limb exoskeleton is operated. The control action is achieved every 2 ms to secure proper control performances.

Fig. 10 presents the block diagram for driving the upper-limb exoskeleton robot. The velocity tracking torque controller based on the *PI* (Proportional–Integral) control produces the torque control input to the actuators, which generates the actuator torque. The detail of the velocity tracking control is explained in Fig. 11. Human force intension F_h operates as the input to the robot and is also generate human torques τ_h. The position of end-effectors and the angle position of joints are denoted p and θ, respectively. The gravity compensation to support the robot frame weight and real-time refractory load-compensation were also applied to the control. The external torque input τ_{ext}, which is added to the actuator, is calculated by measuring the external force from the refractory F_{ext}.

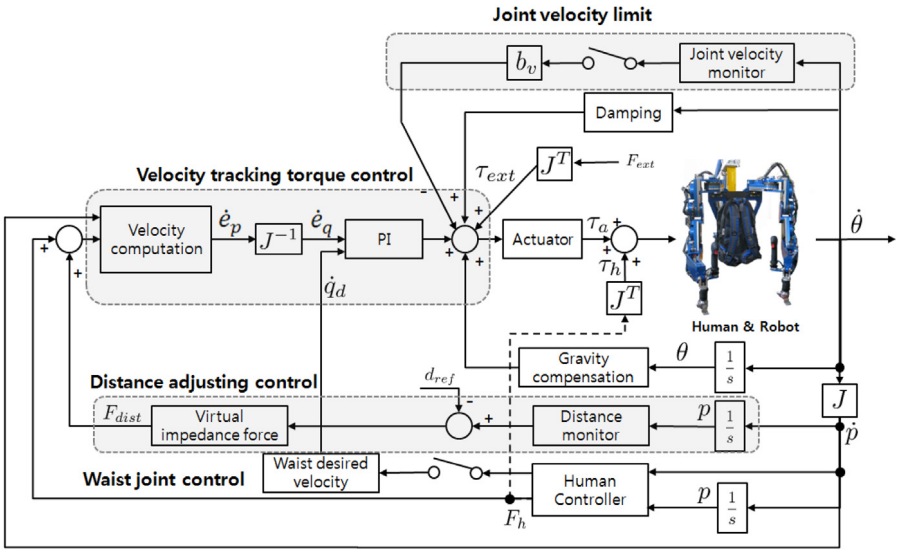

Fig. 10. Control block diagram for upper-limb exoskeleton robot.

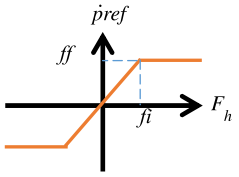

Fig. 11. Hypothetical velocity reference profile.

Additionally, the distance adjusting algorithm, which monitors distance between end-effectors of both arms and keeps the distance constant, was implemented. The distance adjusting forces F_{dist} are generated and control the distance between end-effectors with respect to the reference distance d_{ref}. For the safety, the limits of joint angle were imposed. The damping coefficient b_v hinders motions of the robot in the out of range.

In the velocity tracking torque control, the hypothetical velocity reference profile is given as Fig. 11. The desired velocity input $\dot{p}_{ref}$ corresponding to the signal value of a F/T sensor is produced in the Cartesian space. The saturation values of *ff* and *fi* were set to 10 and 8, experimentally. The velocity error in Cartesian space can be defined as follows:

$$\dot{e}_p = \dot{p}_{ref} - \dot{p}. \tag{4}$$

Then, the velocity error in the joint space is computed with the Jacobian inverse, and therefore the position error becomes the integral of the velocity error.

$$\dot{e}_q = J^{-1}\dot{e}_p \tag{5}$$

$$e_q = \int \dot{e}_q. \tag{6}$$

The joint torque input is presented as the *PI* controller with the damping and gravity compensation term as follows:

$$\tau = k_v\dot{e}_q + k_p e_q + k_d\dot{q} + g\,(q) \tag{7}$$

where k_v, k_p, k_d, and g are the velocity term proportional gain, position term integral gain, damping gain, and gravity compensation torque, respectively.

PI controller gains were set to allow the controller not to respond to trivial velocity errors sharply. It is to obtain the robustness against the F/T sensor noise. The low-pass filter can be used to suppress the sensor noise, but it causes the delay of the signal simultaneously. Therefore, the gains of the tracking controller can be set by considering both fast tracking and robustness. As a result, we established a fast enough and robust controller without the use of filters accompanying delay. Also the damping term was implemented to the joint torque input for stable driving and anti-vibration. The gravity compensation term with respect to the real-time robot posture is added too. In case the refractory is absorbed, the lifting force against the refractory weight via load cells is generated and combined to the joint torque input. This controller does not require the calibration of sensor values so that it has an additional advantage of the maintenance.

4.2. Safety control

The wearable exoskeleton robot cooperates with a human who is positioned and operates it inside the platform so that the safety of the operators is crucial. When the robot malfunctions, the operator may be placed in dangerous condition in case of holding the refractory in particular. Thus, several safety-related control techniques such as an anti-singular motion algorithm, an distance adjusting algorithm, and setting of the joint motion limits were applied.

When robot joints approach the kinematic singularity, singular values of the Jacobian matrix became so small causing the rapid growing of the Jacobian inverse matrix. Physically, this malfunction happens around the kinematic singularity regardless of human's intention. In order to avoid this phenomenon, we used the damped least-squares method, which enables to prevent joint velocity divergence (Chiaverini & Siciliano, 1994; Wampler, 1986).

There are following relations between the velocity in Cartesian space and the joint angle velocity in joint space.

$$\dot{p} = J\dot{q} \tag{8}$$

$$\dot{q} = J^{-1}\dot{p}, \tag{9}$$

where $\dot{p}$ and $\dot{q}$ represents the velocity in Cartesian space and joint angle velocity, respectively. The singular value decomposition of the Jacobian matrix is expressed as follows,

$$J = U\Sigma V^T,\ VV^T = I,\ U^TU = I \tag{10}$$

$$J^{-1} = V\Sigma^{-1}U^T \tag{11}$$

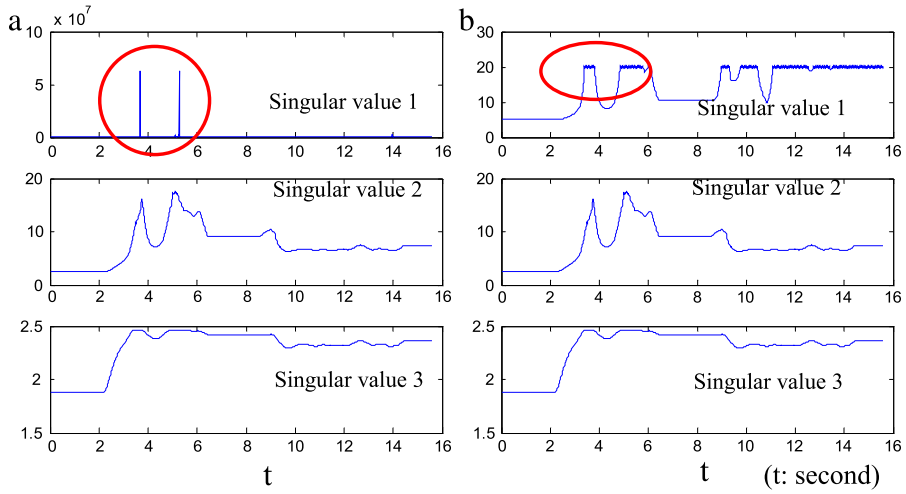

Fig. 12. Simulations of the damped least-squares: (a) the singular values of Jacobian inverse and (b) the singular values of the damped least-squares Jacobian inverse.

where U and V are the input and output singular vectors, respectively. Σ is the singular value matrix. The damped least-squares solution is described by

$$\dot{q} = \left(J^T(q)J(q) + \lambda^2 I\right)^{-1} J^T(q)\dot{p}. \tag{12}$$

The solution satisfies the following condition,

$$min_{\dot{q}}\left(\|\dot{p} - J(q)\dot{q}\|^2 + \lambda^2\|\dot{q}\|^2\right) \tag{13}$$

where λ is the damping factor and I is the identity matrix. The value of damping factor is going to be positive. If the damping factor is zero, the solution (12) is identical condition with the Eqs. (9). The modified Jacobian through the damped least-squares scheme is denoted as J'. Then, the singular value decomposition of J' is derived as

$$J' = U\Sigma' V^T \tag{14}$$

$$\Sigma'_{i,i} = \frac{\sigma_i^2 + \lambda^2}{\sigma_i} \tag{15}$$

where σ_i are the singular values. The modified Jacobian inverse is

$$J'^{-1} = V\Sigma'^{-1}U^T \tag{16}$$

$$\Sigma'^{-1}_{i,i} = \frac{\sigma_i}{\sigma_i^2 + \lambda^2}. \tag{17}$$

Fig. 12 presents the simulation result of the damped least-squares. When the robot joint approaches the kinematic singularity, the singular value of Jacobian inverse became large in Fig. 12(a). On the other hand, the singular value of the damped least-squares Jacobian inverse shows robustness to the occurrence of the singularity. By tuning proper damping factors, the optimized performance of robot can be obtained.

The upper-limb robotic exoskeleton uses a single vacuum gripper to raise the efficiency of refractory transferring operation. This means that both arms are constrained by the rigid gripper in Fig. 9(b). If each arm operates separately by individual F/T sensor signals in the condition of the kinematic constraint, the robot may malfunction resulting in dropping of the refractory, damage of the load cells by unexpected external forces, etc. Thus, we developed the distance adjusting algorithm, which maintains a constant displacement between end-effectors of each arm.

The basic concept of the algorithm is to compensate the distance error by using the virtual impedance. The distance vectors of $\vec{p}_l$ and $\vec{p}_r$ based on the shoulder joints can be derived from the forward kinematics in Fig. 13(a). $\vec{p}_{r'}$ is described with the distance vector between both shoulder joints of $\vec{p}_{shoulder}$.

$$\vec{p}_{r'} = \vec{p}_{shoulder} + \vec{p}_r \tag{18}$$

$$\vec{p} = \vec{p}_l - \vec{p}_{r'}, \tag{19}$$

where $\vec{p}$ is the distance between end-effectors. The distance adjusting algorithm consists of two parts, which are distance controls of z-direction and xy-plane. The heights of both arms are controlled with the virtual impedance to maintain level of the gripper in Fig. 13(b). The vertical adjusting force is given by

$$\vec{F}_{r_z} = K\frac{\vec{p}_{r_z} - \vec{p}_{l_z}}{2} + D\frac{1}{2}\frac{d}{dt}\left(\vec{p}_{r_z} - \vec{p}_{l_z}\right) \tag{20}$$

where K and D are the spring and damping coefficients, respectively. $\vec{p}_{l_z}$ and $\vec{p}_{r_z}$ are the vertical positions of left and right end-effectors, respectively. Similarly, the horizontal distance adjusting force in Fig. 13(c) is described by

$$F = K\left(d_0 - d\right)\frac{\vec{p}_{lr}}{|\vec{p}_{lr}|} + D\frac{d}{dt}\left(d_0 - d\right)\frac{\vec{p}_{lr}}{|\vec{p}_{lr}|} \tag{21}$$

where d and d_0 are the distance between both end-effectors and the desired distance in xy-plane, respectively. The position vector between the left and the right end-effector in xy-plane is denoted as $\vec{p}_{lr}$.

Besides anti-singular motion algorithm and the distance adjusting algorithm described above, the joint angle limits on each joint both in hardware and software were implemented in order to secure the safety in case of the emergency.

5. Experimental results

This section presents experimental results of the upper-limb exoskeleton robot. The simulated converter for the refractory construction was installed in Fig. 14 with the same size as the actual converter. The applicability of the upper-limb exoskeleton robot was verified through numerous demonstrations of refractory construction process. The simulation included the repetitive refractory lifting, transferring, and aligning motions. When the operator wearing the exoskeleton robot transfers the refractory below 50 kg, no load is applied to the operator. Moreover, with the aid of the air-balancer the operator with the upper-limb robot can walk around inside the simulated converter without the lower-limb robot.

The transferring operation with gripping a refractory to the left and right was implemented in Fig. 15. This motion is required mainly when performing the horizontal transferring of the refractory for the short-range construction as described in Section 2. The three dimensional motion of the left end-effector trajectory is given in Fig. 15(a). The x, y, and z-directional travel distances of the end-effector are presented in

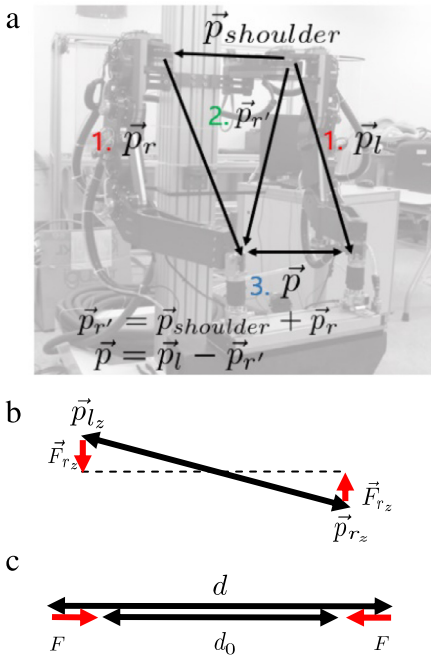

Fig. 13. Distance adjustment between end-effectors: (a) distance vectors, (b) the vertical distance adjusting force generation, and (c) the horizontal distance adjusting force generation.

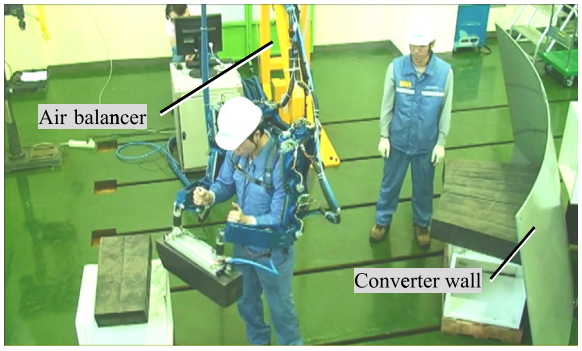

Fig. 14. The simulation of refractory construction operations.

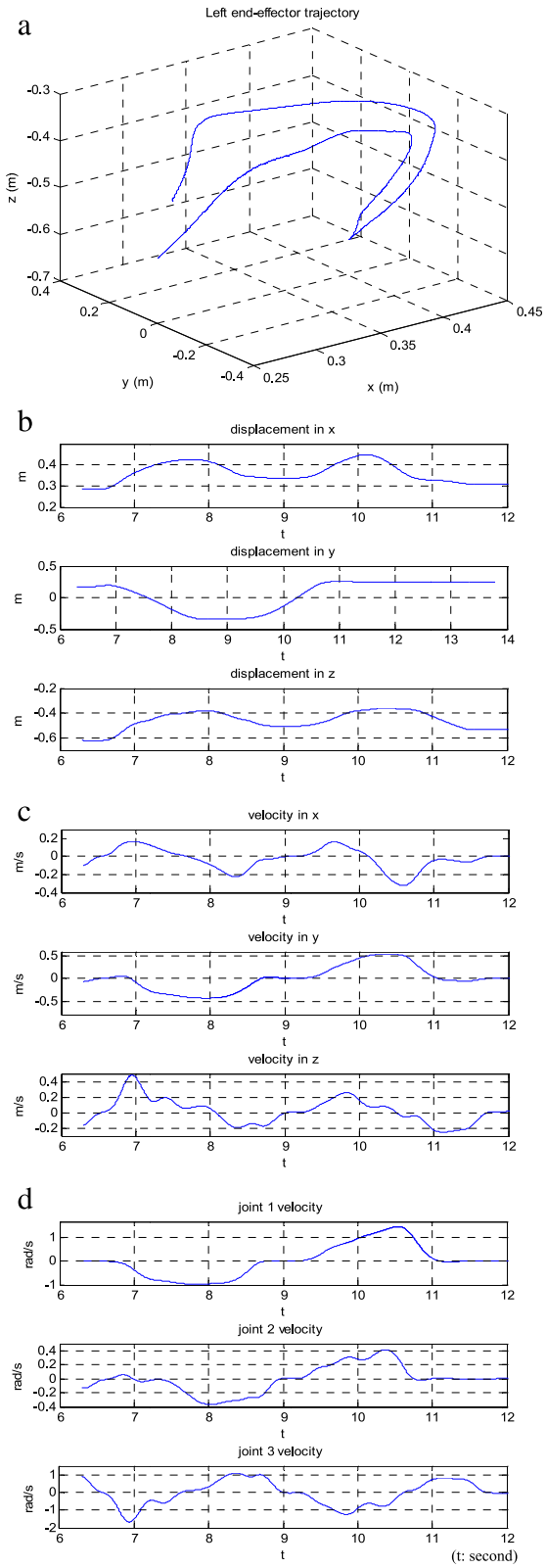

Fig. 15. Refractory transferring operation to the left and right.

Fig. 15(b). Since the left and right motion has been performed, it shows the max movement of 0.6m in y. The x, y, and z-directional velocity of the end-effector are shown in Fig. 15(c). When the robot moves to the left and right, it can be seen that the end-effector has −0.31~0.18 m/s in x, −0.49~0.51 m/s in y, and −0.25~0.49 m/s in z. The maximum velocity was generated on the y-axis, because the operation is mainly performed in the left and right direction. Fig. 15(d) presents each joint angular velocity. The result shows −0.97~1.5 rad/s on the elbow, −0.38~0.41 rad/s on vertical shoulder, and −1.68~1.08 rad/s on the horizontal shoulder. It did not generate the maximum velocity because of the inertia from links and drive modules. The horizontal shoulder joint moved at the highest angular velocity while transferring operation tests. Nevertheless, the refractory transferring operation is dependent on the operator wearing the robot so that the result can be varied through operators.

The refractory construction work requires not only the horizontal refractory transport motion above but also more complicated motions mixed with horizontal, vertical, and rotational motions for refractory alignment. Hence, dual arms in the upper-limb exoskeleton robot should be able to generate three dimensional movements freely utilizing multi-degree-of-freedom joints as shown in Fig. 16(a). The x, y, and z-directional travel distances of the end-effector are shown in Fig. 16(b). Around 200 mm diameter rotation motion in lateral and the movement

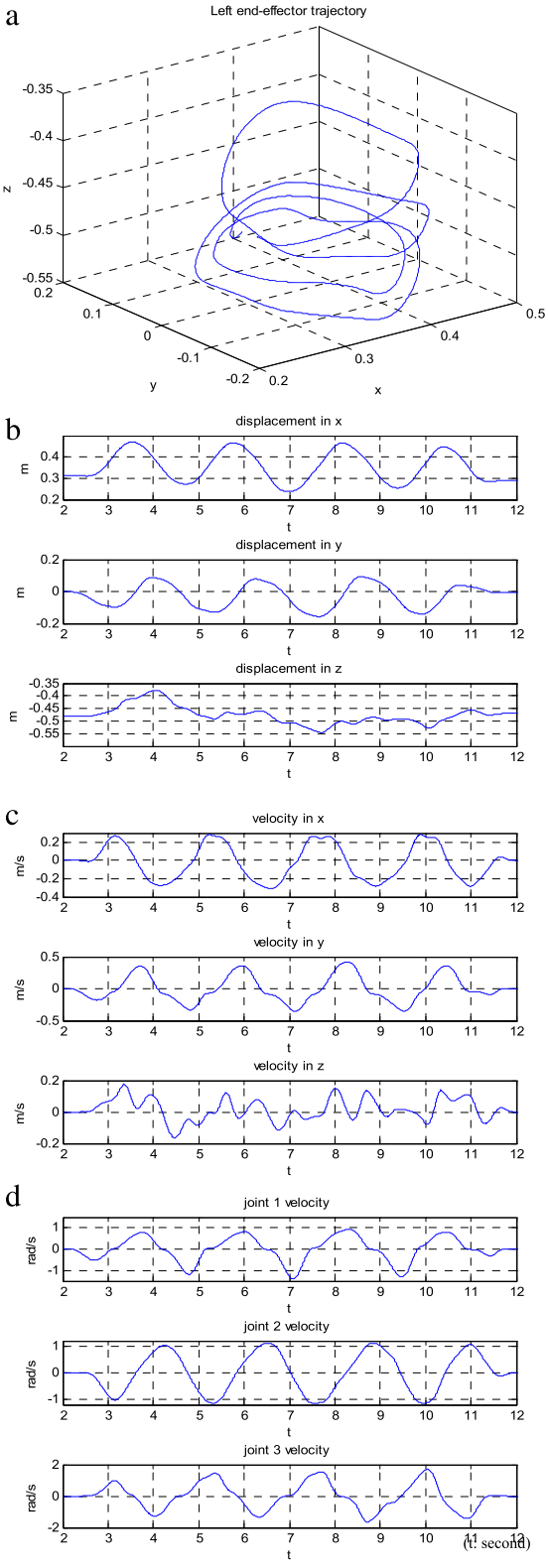

Fig. 16. Three dimensional movement of the end-effector.

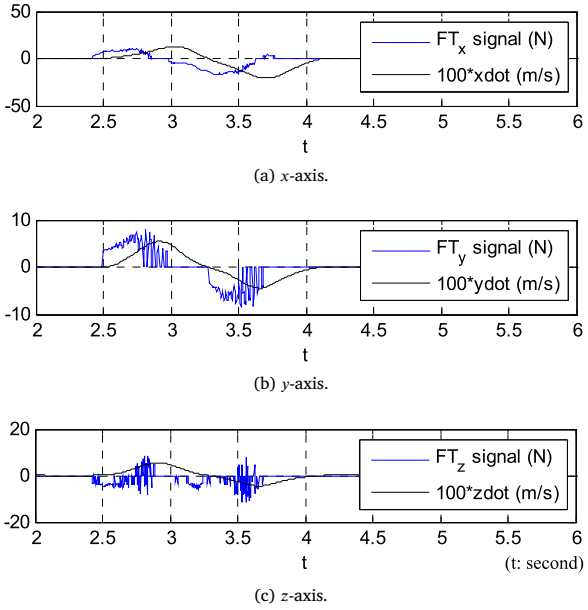

Fig. 17. Relations between F/T sensor signals and velocities of the end-effector.

of the direction of gravity were included when we demonstrated the spring motion. The x, y, and z-directional velocity of the end-effector are presented in Fig. 16(c). The end-effector moved in the range of −0.28~0.29 m/s in x, −0.31~0.42 m/s in y, and −0.16~0.17 m/s in z. Fig. 16(d) shows each joint angular velocity, which shows −1.32~0.88 rad/s on the elbow, −1.15~1.17 rad/s on vertical shoulder, and −1.64~1.85 rad/s on the horizontal shoulder. The result explains that the exoskeleton robot can perform sophisticated operations such as aligning, sorting, and gripping in various positions and angles. The right arm also shows identical performances with the left, and the combination of both arm motions can produces diverse postures for refractory constructions.

The exoskeleton robot is driven by the electric actuators using the input from F/T sensor signals created by the operator. The velocities of the end-effector in x, y, and z-direction as dotted lines against F/T sensor signals as solid lines are described in Fig. 17. In order to facilitate comparison between both signals, we considered the scale factors of 100 in velocities of the end-effector. It is shown that the suitable dynamic response between the sensor and actuators is achieved by virtue of the velocity tracking torque control. The excessively sensitive or slow and blunted reactions may cause discomfort to the user. In the figure, the control does not allow the severe delay at start points of the movement while the trivial delay exists by means of the inertia of robot frame and artificial damping incorporated into the control. The amount of delay and the velocity of the robot joints can be increased by adjusting the parameters of the tracking torque control. However, the sensitivity of motions is determined experimentally by the consideration of the safety with the load and the preference of operator.

The air-balancer ensures the freedom of horizontal motions. Since no external force is applied in the horizontal direction in an ideal environment, only the force to overcome the inertia of mass is required to move the robot horizontally. However, the air-balancer sometimes does not maintain the level of horizontality fully in the real environment. Due to the repetitive heavy weight loading, the links of the air-balancer are tilted a little. Then, the weight of refractory and robot frame cause leaning to one side, and this disturbs the walking motion of the operator. It is necessary to maintain the level consistently for the smooth operation of the robot system.

6. Conclusion

Operators who perform the refractory construction of the converter in steel-making process are suffering from muscle pains on the waist and wrists due to a long period of work with heavy weights. In order

to relieve the operators' load and avoid the safety accidents, the upper-limb exoskeleton robot was developed and applied successfully to the refractory construction work at the simulated worksite in POSCO.

Experimental results demonstrated that the robot can handle a maximum 50 kg refractory and act various motions required to move refractories. Moreover, the upper-limb exoskeleton robot can be used without the lower-limb by utilizing the air-balancer, which is the existing equipment in the worksite. The air-balancer could generate a great movement ability in the limited working space for a repetitive operation such as the refractory construction. The F/T sensors were used to recognize the wearer's motion intension easily and intuitively. In addition, the robust velocity tracking torque control and several safety controls enabled operators to perform refractory transferring operations without inconveniences and safety accidents.

Apart from refractory constructions in various sorts of furnaces, the exoskeleton robot technology can be usefully employed to the diverse applications in POSCO such as hand scarfing, balance-weight moving for the load cell calibration, the maintenance of tundishes and ladles, etc. Furthermore, this technology can be extended to various fields such as building construction, logistics, military, health care and so on.

References

Chiaverini, S., & Siciliano, B. (1994). *IEEE Transactions on Control Systems Technology*, *2*, 123.

Daewoo Shipbuilding and Marine Engineering (DSME), (0000). URL: http://www.dsme.co.kr, [Online] Available at: (http://spectrum.ieee.org/automaton/robotics/industrial-robots/korean-shipbuilder-testing-industrial-exoskeleons-for-future-cybernetic-workforce).

Hayashi, T., Kawamoto, H., & Sankai, Y. (2005). In *IEEE/RSJ international conference on intelligent robots and systems*, (p. 3063).

Huang, L., Steger, J. R., & Kazerooni, H. (2005). In *ASME international mechanical engineering congress and exposition*, Orlando, (p. 1).

Hyundai Motor Group, (0000). URL: http://www.hyundai.co.kr [Online] Available at: (http://www.4erevolution.com/en/hyundai-entre-dans-la-course-vers-lexosquelette-industriel/).

Kawabata, T., Satoh, H., & Sankai, Y. (2009). In *IEEE international conference on robotics and biomimetics*, Guilin, (p. 2013).

Kazerooni, H., Racine, J. L., Huang, L., & Steger, R. (2005). In *IEEE International conference on robotics and automation*, Barcelona, (pp. 4364).

Lockheed martin, (0000). URL: www.lockheedmartin.com.

Mosher, R. S. (1967). *SAE Automotive Engineering Congress, Vol. 670088*. Detroit.

Raytheon, (0000). XOS [Online] Available at: (http://www.raytheon.com).

ReWalk Robotics, (0000). URL: www.rewalk.com.

Vicon, (0000). [Online] Available at: (http://www.vicon.com).

Wampler, C. W. (1986). *IEEE Trans. Syst. Man Cybern.*, *16*, 93.